Demonstration of Anisotropic Composites with Tuneable Microwave Permeability Manufactured from Ferromagnetic Thin Films

Olivier Acher, Pierre Le Gourriérec, Géraldine Perrin, Philippe Baclet, and Olivier Roblin

Abstract—**Recently, we presented the microwave properties of laminated insulator ferromagnetic on the edge (LIFE) composites. For the fundamental mode propagating in a coaxial line, they exhibit large permeability and low permittivity. In this paper we investigate the properties of LIFE composites in the 0.1 to 18 GHz range when a static magnetic field is applied along the propagation direction. We show that the evolution of the resonance frequency with the external field can be described by conventional gyromagnetic resonance models. The effect of demagnetizing fields is analyzed. In particular, it is shown that LIFE materials exhibit comparatively low demagnetizing effects and large permeabilities. The evolution of the resonance linewidth with the external field is investigated. LIFE material may be used for a variety of microwave applications in a coaxial line or in a guide. In particular, we demonstrate a tuneable coaxial absorbing termination with peak attenuation frequency tuneable from 1.7 to 18 GHz with more than −15 dB maximum attenuation, and a switchable termination that can be either reflective or absorbing. The operation of a field-driven variable attenuator is also presented.**

I. Introduction

HIGH permeability materials are important for microwave applications. Ferrite and garnets are widely used as high-permeability materials. They generally exhibit intrinsic impedances $Z = \sqrt{(\mu/\epsilon)}$ larger than unity over a wide frequency range. In contrast, ferromagnetic materials have limited applications as microwave materials. Because of their large conductivities, they exhibit very large permittivities and microwaves hardly penetrate into bulk ferromagnetic materials. Ferromagnetic materials are widely used for electrical engineering applications such as inductors [1] or magneto-inductive recording heads [2]. In these applications, thin ferromagnetic films are widely appreciated as high permeability materials, and in many cases they exhibit better figure of merits than ferrimagnetic materials. However, the use of thin ferromagnetic films or laminations has been restricted to our knowledge to cases where the magnetic field is generated inside the lamination by a surrounding coil or yoke. It has been for long recognized that it would be attractive to take advantage of the high microwave permeabilities of ferromagnetic thin films for guided or free space applications [3]. One well-known way to turn metallic materials into microwave materials is to manufacture a composite by dispersing ferromagnetic particles in an insulating binder. It is necessary that at least one dimension of the particles is very small, so that the wave penetrates in the metal. The microwave properties of composites manufactured from ferromagnetic powders have been reported [4]. However, the permeability of these composites is lower than their permittivity over the whole frequency range.

The geometry of the composite and that of the ferromagnetic inclusions are clearly key features for the permeability and permittivity of the composite. There are some hints that it is difficult to obtain a composite with intrinsic impedance larger than unity, whereas both matrix and ferromagnetic inclusions have an intrinsic impedance lower than unity.

Recently, we proposed a way to obtain ferromagnetic-based composites with intrinsic impedance larger than unity for one polarization [5]. These composites were denominated laminated insulator ferromagnetic on the edge (LIFE) materials [6]. Experimental measurements of permeability and permittivity for this polarization were in good agreement with our predictions. In this paper we investigate the microwave properties of LIFE composites under external magnetic field. This experiment has some similarities with conventional ferromagnetic resonance (FMR) measurements. However, in contrast with classical FMR, our technique allows the investigation of microwave permeability on a wide frequency band, and in both the saturated and unsaturated regime.

II. Description of Life Geometry

A. Presentation

Let us consider the lamination sketched on Fig. 1. It consists in alternated ferromagnetic and insulating thin sheets placed on the edge. This structure is called LIFE [5], [6]. It is clearly an anisotropic composite. The two eigenpolarizations for a propagation vector normal to the LIFE surface (and therefore parallel to the lamination plane) correspond to the electric field $\boldsymbol{E}$ parallel and normal to the lamination plane, respectively. The material behaves as a plain conductor for $\boldsymbol{E}$ parallel to the lamination. In contrast, it is intuitive that for the other eigenpolarization ($\boldsymbol{E}$ perpendicular to the laminations and the magnetic field $\boldsymbol{H}$ parallel to the laminations), the material behaves as a low permittivity, high permeability material. This can be shown rigorously: Wiener's laws [7] describe these composites if the ferromagnetic layer thickness is much smaller than skin depth, and the insulator thickness is much

Manuscript received June 10, 1995; revised January 17, 1996.

The authors are with CEA, DETN, Centre d'Etudes de Bruyères le Châtel, BP12 F-91680 Bruyères le Châtel, France.

Publisher Item Identifier S 0018-9480(96)03024-4.

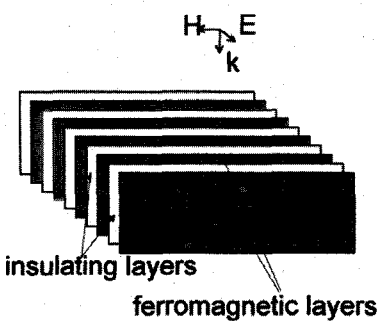

(a)

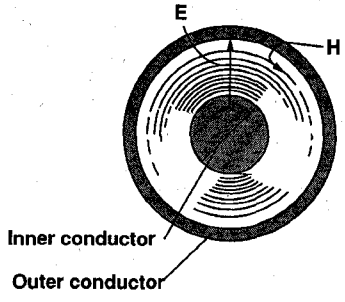

(b)

Fig. 1. Sketch of a LIFE composite. (a) Adapted to free space propagation. The working polarization is indicated, (b) adapted to coaxial line operation. H and $\boldsymbol{E}$ fields for the fundamental mode are sketched.

smaller than the wavelength inside the composite. For the eigenpolarization H parallel and $\boldsymbol{E}$ normal to the lamination plane, it writes

$$\mu_{\text{eff}} = f_c\mu_c + (1 - f_c) \Leftrightarrow (\mu_{\text{eff}} - 1) = f_c(\mu_c - 1) \quad \text{(1a)}$$

$$\epsilon_{\text{eff}} = \frac{\epsilon_i}{f_i}. \quad \text{(1b)}$$

The eff subscript is related to the properties of the composite, the c subscript to the conducting ferromagnetic layer and i to the insulator. f_c is the ferromagnetic volume fraction in the LIFE material. When ferromagnetic thickness is not small compared to skin depth, Rytov [8] equations can describe LIFE composites. For small insulator thickness, they write

$$\mu_{\text{eff}} = \frac{f_c C_c \mu_c + f_i}{(1 + f_c(C_c - 1))} \quad \text{(2a)}$$

$$\epsilon_{\text{eff}} = \frac{\epsilon_i}{f_i}[1 + f_c(C_c - 1)] \quad \text{(2b)}$$

with

$$C_c = \frac{\tan X}{X} \quad \text{and}$$

$$X = \frac{k_c e_c}{2} = e_c\sqrt{\frac{\pi}{2}\sigma F \mu_0(-j\mu_c)} \quad \text{(2c)}$$

k_c is the wavevector in the ferromagnetic material, σ its conductivity, F the frequency and μ_0 the void permeability.

B. Measurement Procedure

The determination of microwave properties of anisotropic materials is a complex problem [9]. In the case of LIFE materials, our interest is mainly in measuring the component $\mu_{//}$ and $\epsilon_\perp$ of permeability and permittivity tensor corresponding to the eignepolarization sketched on Fig. 1(a). Even this problem has no trivial solution. Free-space measurements would require very large size samples. Reflection-transmission measurements in wave guides can be made, but they require quite large samples, and they cover a very limited bandwidth. Reflection-transmission measurements in coaxial line are extremely popular for determining the radioelectric properties of isotropic materials [10], because they yield wide-band (typically 50 MHz to 18 GHz) measurements and require small size samples. However, coaxial measurements are not adapted to measurements on composites that are anisotropic in the plane normal to the wave vector. Cutting a torus in the material of Fig. 1(a) parallel to the surface and performing a coaxial line measurement would lead to no intelligible data.

As a consequence, we proposed [5] and [6] to adapt the geometry of the LIFE composite to that of the electromagnetic field in the coaxial line. For the fundamental mode, the electric field is radial, and the magnetic field orthoradial. A sample consisting in alternated concentric ferromagnetic and insulating layers will interact with a wave that has its electric field normal to the laminations, and its magnetic field parallel to the laminations. A rigorous analysis of this geometry [11] leads to the same expressions of $\mu_{//}$ and $\epsilon_\perp$ as (2), provided the sample is finely laminated. In practice, torus with proper geometry are manufactured by winding ferromagnetic films deposited on thin flexible substrates [12]. The differences between measurements performed on the concentric geometry and these made on spiral-like geometry were shown to be negligible on the permeability [6], and generally small on the permittivity [5].

The measurement of the permeability of LIFE composites allows the determination of the intrinsic permeability of the ferromagnetic constituent through (1) or (2) as in [6]. As a consequence, experimental results can be presented under two dual forms, in terms of permeability of either the composite or the layer. In this work, the results are presented in terms of properties of the composite.

III. Experimental Detail

Amorphous cobalt-based materials are deposited onto continuously transported mylar films by magnetron sputtering [12]. These materials are known to have good soft magnetic properties [13] and moderate to nearly zero magnetostriction.

The thickness of the layers is determined from scanning electron microscopy observations. Saturation magnetization of the films is measured using a magnetic balance, or deduced from tabulated values [14]. A 50 Hz coil hysteresimeter is used to investigate B-H loops. Permeability is measured from 20 MHz up to 3 GHz on 9×9 mm^2 samples using a permeameter described elsewhere [15]. The deposits have uniaxial in-plane anisotropy. The easy axis is oriented along the film transport direction, except on the edges of the film where the direction of anisotropy is perturbed. The uniform orientation of the easy axis on most of the film surface is due to the influence of the stray static magnetic field of the planar magnetron. The

TABLE I
CHARACTERISTICS OF THE DIFFERENT SAMPLES UNDER INVESTIGATION

Sample No	layer composition	4.pi.Ms (layer) (kG)	fc.4.Pi.Ms (G)	ferro. vol. fraction fc (%)	torus thickn. (mm)	permeability along:
A	CoZrMoNi	7.5	305	4.1	1.45	hard axis
B	CoZrMoNi	7.5	270	3.6	1.98	hard axis
C	CoNbZr	10.7	231	2.2	2.48	easy axis
D	CoNbZr	10.7	218	2.0	2.6	easy axis

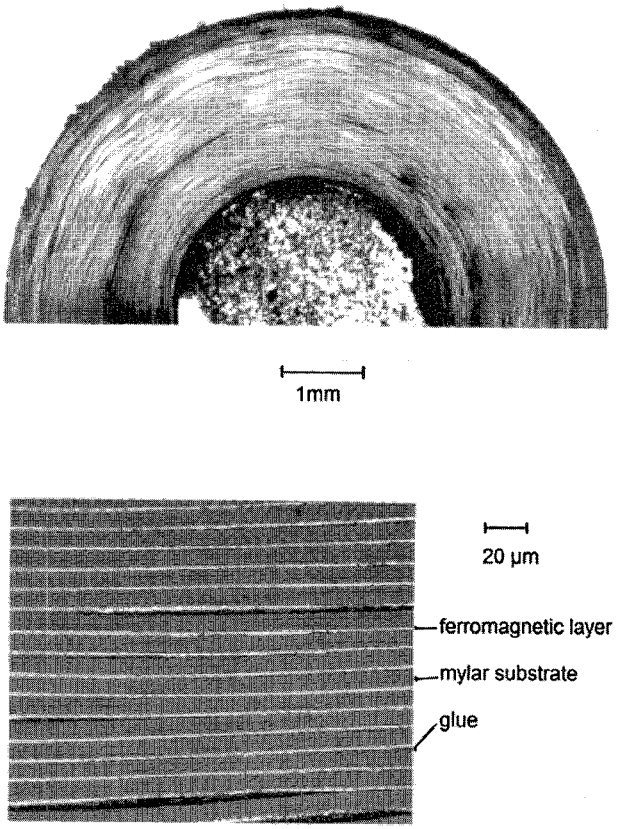

Fig. 2. Picture of a LIFE torus adapted to coaxial line measurements.

horizontal component of the magnetic field of the magnetron lies in the transport direction, except on the edges [12].

Dynamic permeability along transport direction (i.e., along easy axis) is found to be close to unity, whereas dynamic permeability normal to the transport direction (i.e., along hard axis) has large values and exhibits resonant behavior. This indicates that the origin of microwave permeability on these films is rotational permeability and not domain wall permeability. In this paper, two films are investigated. One 0.4 μm thick amorphous $Co_{79}Zr_{10}Mo_9Ni_2$ (at%) with saturation flux density of 7.5 kG was deposited on 8 μm thick mylar film, and one 0.5 μm thick amorphous $Co_{87}Nb_{11.5}Zr_{1.5}$ with saturation flux density of 10.7 kG film was deposited on 12 μm thick mylar. For each film, ribbons were cut along the hard axis (which is the high permeability direction), and wound and glued into a torus. The torus was then machined to the precise dimensions of a APC-7 coaxial line (7 mm outer diameter and 3.04 mm inner diameter) with standard tolerances [16], and parallel faces (see Fig. 2). Torus thicknesses are in the 1 to 3 mm range. Other torus were manufactured from ribbons cut along the easy axis, which is also the low permeability direction. The saturation magnetizations of the torus are measured using a B-H hysteresimeter. The ferromagnetic volume fraction in each torus is deduced from these measurements. The characteristics of the different samples are summarized in Table I.

Microwave measurements on the samples are performed using a standard coaxial fixture and a network analyzer, following a well-tried procedure [16]. In particular, the signals transmitted and reflected by the sample are recorded both when the wave goes from port 1 to port 2 of the network analyzer, and from port 2 to port 1. A static magnetic field can be applied along the torus axis (i.e., the propagation direction). For that purpose, we use an electro-magnet with hollow iron poles so that the coaxial line can go through the poles and along the field axis. The electro-magnet was calculated so that the field inhomogeneities did not exceed 5% in the zone containing the sample. The residual magnetic field induced by the remanent magnetization of the iron poles is about 60 Oe, and field at maximum allowed intensity in the electro-magnet is 5 kOe.

IV. EXPERIMENTAL RESULTS

A. Permeability and Permittivity Measurements

1) Sample with High Permeability in the Demagnetized State: The microwave properties of LIFE sample A under various static fields are indicated on Figs. 3 and 4. The permeability is clearly affected by the static magnetic field, since the resonance frequency goes from 1.7 GHz up to more than 18 GHz. In contrast, the permittivity is not affected by the external field, except some perturbations near the resonance frequency. Sample B exhibits a very similar behavior. The resonance on the permeability curve shifts to higher frequency when the external field is applied.

2) Sample with Low Permeability in Demagnetized State: The microwave properties of LIFE sample C under various static fields are indicated on Figs. 5 and 6. In contrast with sample A and B, the gyromagnetic permeability in the absence of field is quite low. This is because the local magnetization in the sample is orthoradial, that is parallel to the microwave magnetic field. Indeed, the permeability would be expected to be unity in the investigated frequency range if all the ferromagnetic domains were perfectly oriented parallel to the torus plane. At low field [see Fig. 5(a)], the effect of the field is to increase the permeability without hardly changing the resonance frequency. At higher field [see Fig. 5(b)], the behavior of the permeability with H_{ext} is similar to that of sample A. Increasing the external field H_{ext} increases the resonance frequency and decreases permeability levels. The

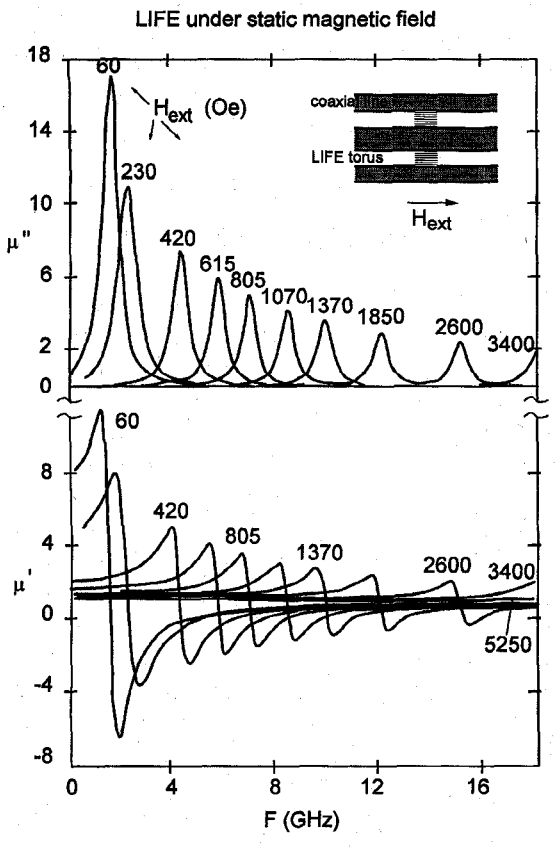

Fig. 3. Microwave permeability of sample A under various static magnetic fields (field indicated in Oe).

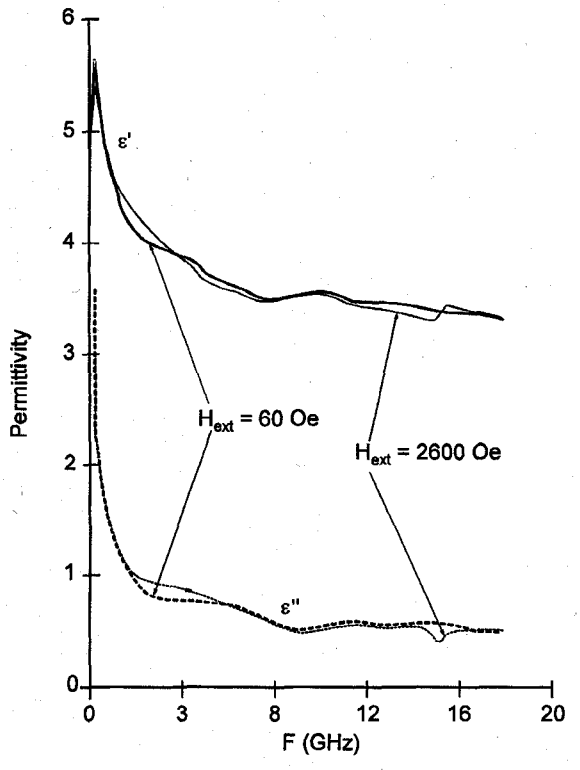

Fig. 4. Microwave permittivity of sample A for a bias field of 60 Oe and 2600 Oe.

permittivity is hardly affected by the field, as can be seen on Fig. 6. Sample D has essentially the same features, except that it has a still lower permeability level under zero field (Fig. 7). Its imaginary permeability is less than 0.7 at all frequencies, whereas the imaginary permeability of sample C under zero field is 2.3. Ferromagnetic volume fraction is similar on both samples. As a consequence, sample D appears better oriented than sample C.

B. Behavior as Antireflection Termination

1) Samples with High Permeability in the Demagnetized State: Sample A was placed on a metallic short in the coaxial line, and the reflection coefficient S_{11} was measured. Its module is represented on Fig. 8. The sample thickness ($e = 1.45$ mm) has been chosen so that the material placed on a metallic reflector has good antireflection properties with zero bias field. But the remarkable result contained in Fig. 8 is that the sample retains its absorbing properties for this same thickness even up to 18 GHz, that is more than a decade above the absorbing frequency in the absence of bias. The absorption peak depth always exceeds -15 dB. We have demonstrated an antireflection termination with nearly constant bandwidth, and peak frequency adjustable from 1.7 GHz to 18 GHz or more!

2) Sample with Low Permeability in Demagnetized State: The materials have limited dielectric losses. In the absence of bias field, they also have limited magnetic losses, especially sample D. Their thickness is small compared to wavelength. As a consequence, samples C and D placed in front of a metallic short in a coaxial line hardly affect the reflection coefficient in the absence of external field (Figs. 9(a) and 10). When the external field increases, the material becomes anti-reflective. This is due to the increase in imaginary permeability, as can be seen on Fig. 5. The reflection coefficient of sample C is switched from -1.9 dB to -45 dB at 1.93 GHz at an external field of 137 Oe. In the case of sample D, the reflection coefficient is switched from -0.9 to -39 dB at 1.85 GHz at an external field of 123 Oe. At higher field, the gyromagnetic resonance frequency increases, and the absorption frequency increases accordingly.

C. Behavior as Transmission Variable Attenuator or as High Index Impedance-Matched Material

The reflection and transmission behavior of sample B is investigated in more details. The S_{11} and S_{12} quantities were recorded, as well as the permeability and permittivity deduced from these quantities. They are shown on Fig. 11. In particular, it should be mentioned that under a bias field of 230 Oe, the values of permeability and permittivitty below 1 GHz are very close. At 800 MHz, $\epsilon = 3.44 - j0.17$, and $\mu = 3.24 - j0.27$. The module of the intrinsic impedance is 0.976, that is 2.5% less than that of vacuum. As a consequence the reflection coefficient at the air-material and material-air interface is expected to be nearly zero. In other words, the material is impedance-matched to the vacuum, though its refractive index is much larger than unity: $N = 3.37 - j0.19$. Below 1 GHz, S_{11} at 230 Oe is 15 to 40 dB lower than for a material with the same permittivity and $\mu \approx 1$.

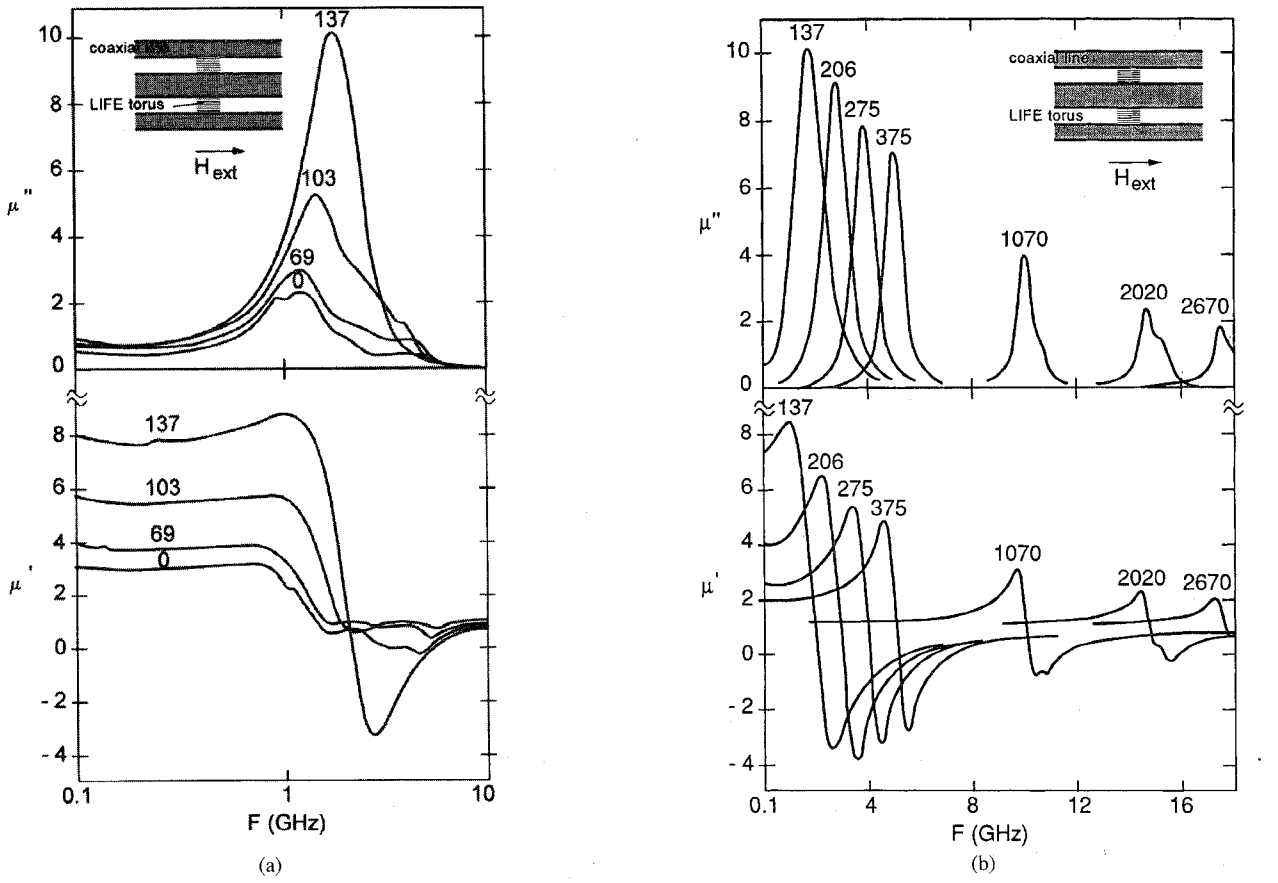

Fig. 5. Microwave permeability of sample C under various static magnetic fields (field indicated in Oe). (a) Low field region. (b) High field region.

V. Discussion

A. Model

1) Origin of the Measured Permeability: The contributions to permeability are generally separated into domain wall movement and gyromagnetic contribution. For a sample with all magnetic domains magnetized along the easy axis and in the film plane, the effects of these two contributions depend on the orientation of the exciting H field in the film plane.The first one contributes to permeability along easy axis, but not along hard axis. On the contrary, gyromagnetic contribution is only along hard axis. Besides, domain permeability loss peak is generally at much lower frequency than that related to gyromagnetic permeability. For the ferromagnetic layers under investigation, the permeability above 100 MHz is essentially along the hard axis, as can be seen from Figs. 3, 5, and 7, and in [6]. Besides, the permeability measurements along the easy axis (see Figs. 5 and 7) reveal loss peaks at essentially the same frequencies as along the hard axis. This suggests that a significant contribution to the residual permeability levels measured along the easy axis may be due to some misorientation of the ribbon used to manufacture the torus, but not to a separate phenomenon. As a consequence, the main contribution to the observed permeability is gyromagnetic. This is coherent with the rather high resonance frequency.

2) Gyromagnetic Resonance Equation: Several models can account for the gyromagnetic permeability [17], [18]. They differ by the phenomenological term used to take the gyromagnetic damping into account. In the case of small RF powers and small damping, they are commonly regarded as nearly equivalent. We chose to use Bloch–Bloembergen model. For a microwave field in the film plane, the permeability along the easy axis $\mu_{\text{e.a.}}$ writes

$$\mu_{\text{e.a.}} = 1 - j.0. \tag{3}$$

It corresponds to a microwave field parallel to the magnetization. If the microwave field is perpendicular to the magnetization, the response of the material is described by the permeability along hard axis $\mu_{\text{h.a.}}$ that writes

$$\mu_{\text{h.a.}} = 1 + \frac{4\pi M_s}{H_{\text{eff}}}\left(1 - \left(\frac{\Delta F}{2F^*}\right)^2\right) \frac{1}{\left(1 - \left(\frac{F}{F^*}\right)^2 + j\frac{\Delta F}{F^*}\frac{F}{F^*}\right)} \tag{4a}$$

where $4\pi M_s$ is the saturation magnetization of the material, H_{eff} is the sum of the static fields exerted on the film, and ΔF is the damping parameter, with

$$F_0^2 = \gamma^2(4\pi M_s + H_{\text{eff}})H_{\text{eff}} \tag{4b}$$

$$F^{*2} = F_0^2 + \left(\frac{\Delta F}{2}\right)^2. \tag{4c}$$

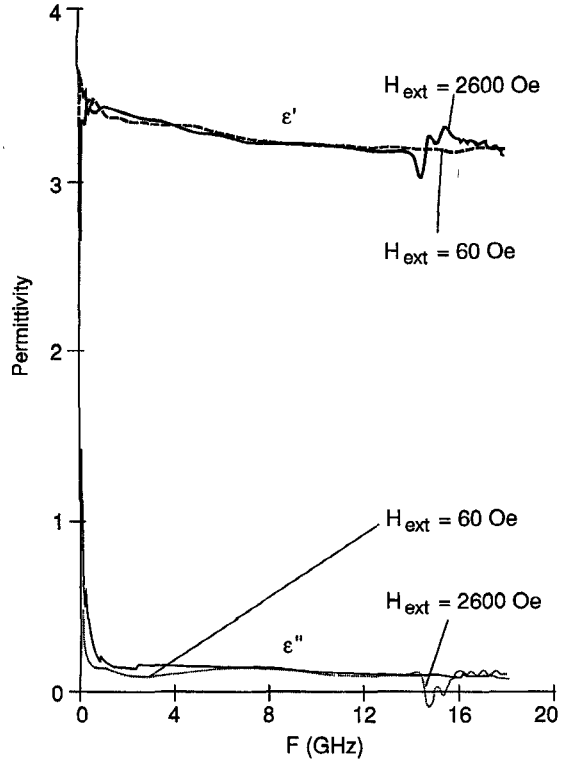

Fig. 6. Microwave permittivity of sample C for a bias field of 60 Oe and 2600 Oe.

F^* is the phase resonance frequency, that is $\mu_{\text{h.a.}}(F^*) = 1 - j0$. $F0$ is the module resonance frequency, that is μ" reaches its maximum at F_0, at least to an approximation order in $(\Delta F/F)^4$. It can also be shown that ΔF is the full width at half maximum of the loss peak, with a very good approximation. Equation (4a) can also be expressed in a more condensed form using relative frequency $\nu = F/F^*$ and relative damping parameter $\beta = \Delta F/F^*$.

If the ferromagnetic layer thickness is small enough, then (1a) and (4a) yield the microwave permeability of the composite along the hard axis $\mu_{\text{c.h.a.}}$

$$\mu_{\text{c.h.a.}} = 1 + f_c \frac{4\pi M_s}{H_{\text{eff}}}\left(1 - \left(\frac{\Delta F}{2F^*}\right)^2\right) \frac{1}{\left(1 - \left(\frac{F}{F^*}\right)^2 + j\frac{\Delta F}{F^*}\frac{F}{F^*}\right)}. \quad (5)$$

The H_{eff} field is the sum of the anisotropy field H_k, of the external field H_{ext}, and of the demagnetizing field H_d

$$H_{\text{eff}} = H_k + H_{\text{ext}} + H_d. \quad (6)$$

The demagnetizing field may not be homogeneous over the sample.

B. Interpretation of the Field-Induced Permeability Shift

1) Procedure: There are two straightforward ways to deduce H_{eff} from the microwave measurements using relations (4) or (5). Using (4b), it is simple to determine H_{eff} from

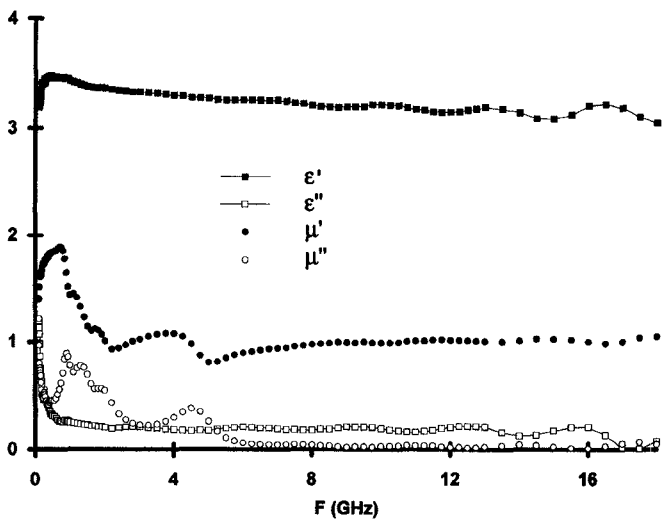

Fig. 7. Microwave properties of sample D without any bias field.

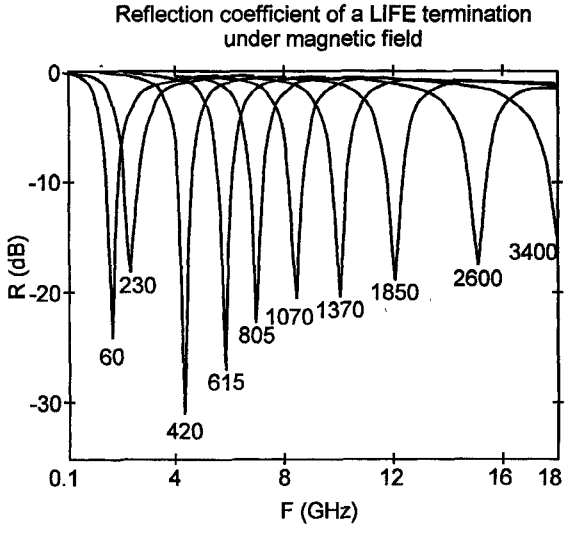

Fig. 8. Reflection coefficient (or S_{11}) measured on sample A placed in contact with a metallic short in the coaxial line, for various external fields.

the measured frequency corresponding to the maximum of permeability loss. It is also possible to note that

$$H_{\text{eff}} = \frac{f_c 4\pi M_s}{(\mu_{\text{c.h.a}}(F = 0) - 1)}\left(1 - \left(\frac{\Delta F}{2F^*}\right)^2\right). \quad (7)$$

The factor containing ΔF is generally a small corrective factor.

When the resonance frequency is below 4 GHz, the low frequency permeability level $\mu(0)$ is extrapolated from the values measured in the 0.1 to 1 GHz frequency range using Bloch–Bloembergen relations. When the resonance frequency is above 4 GHz, the real permeability is very nearly constant up to 1 GHz, and $\mu(0)$ is directly read on the curves. The $f_c 4\pi M_s$ quantity is measured using an hysteresimeter and is indicated on Table I.

The uncertainties on the determination of H_{eff} using (4b) have been computed supposing the uncertainty on $4\pi M_s$ is 6%, and the error on the experimental determination of F_0 is

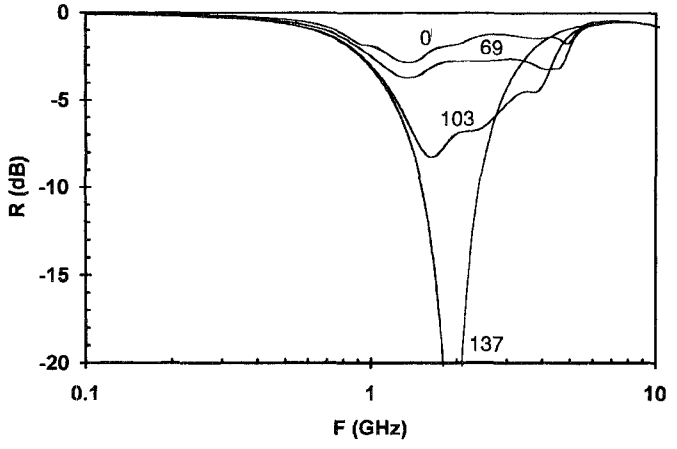

(a)

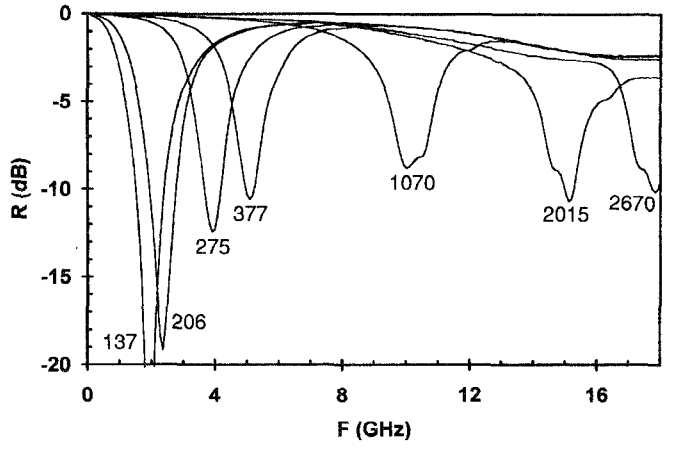

(b)

Fig. 9. Reflection coefficient R (or S_{11}) measured on sample C placed in contact with a metallic short in the coaxial line, for various external fields. (a) Low field region. (b) High field region.

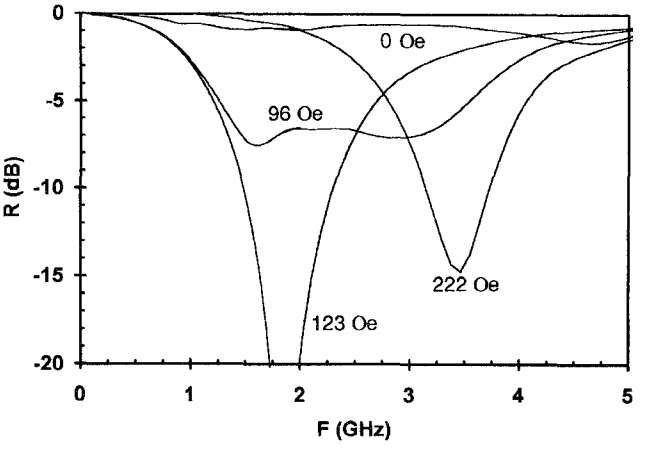

Fig. 10. Reflection coefficient R (or S_{11}) measured on sample D placed in contact with a metallic short in the coaxial line, for various external fields. Only the low-field region is represented.

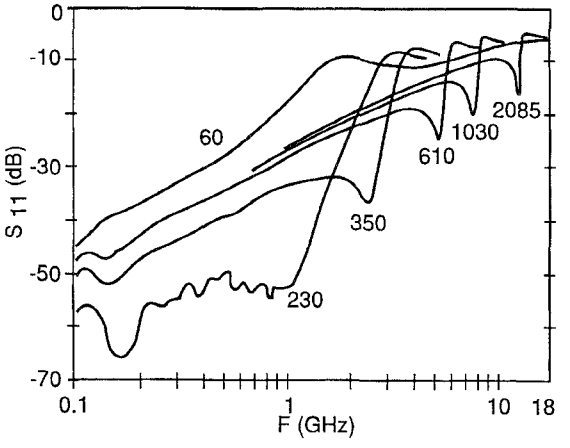

(a)

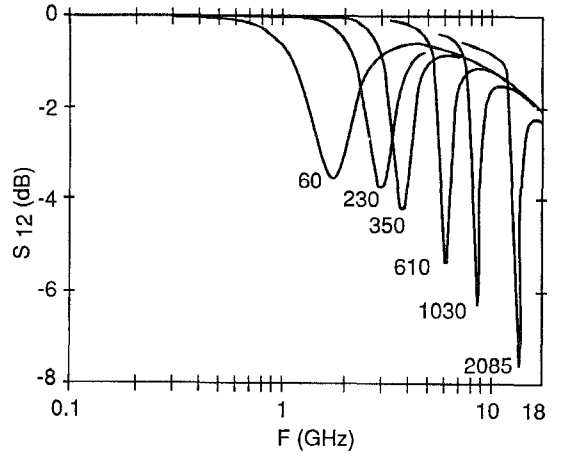

(b)

Fig. 11. Reflection-transmission measurement of sample B placed in the coaxial line. (a) Reflection coefficient S_{11}. (b) Transmission coefficient S_{12}.

0.15 GHz. The uncertainties on the determination using (7) have been determined supposing 6% uncertainty on $f_c 4\pi M_s$ and 5% uncertainty on $\mu(0)$. It should be also reminded that the uncertainty on the external field determination is about 5%.

2) Results: Fig. 12 gives the effective field H_{eff} as a function of the external field H_{ext} for sample A, deduced from the measurements of Fig. 3 from relation (4b) and (7). Fig. 13 gives H_{eff} as a function of H_{ext} for sample B and C deduced from relation (7). In the relation (6) between the external field and the effective field, the point is that the demagnetizing field is unknown. Indeed, it should be stressed that the demagnetizing field is not homogeneous within the sample. It is possible to compute the demagnetizing field in every point of the LIFE structure if the B-H loop of the ferromagnetic layer is known. However, we propose a simpler approach. The demagnetizing field of one layer is expected to be much smaller than its saturation magnetization, because the aspect ratio of one layer is very small. One may approximate the rest of the composite as an homogeneous material with saturation magnetization $f_c 4\pi M_s$. It is known that the demagnetizing field created by an homogeneous ellipsoid is between zero and $-f_c 4\pi M_s$, depending on the geometry. This suggests that the demagnetizing field in most of the torus is between zero and $-f_c 4\pi M_s$.

The characterization procedure of ϵ and μ in a coaxial line requires that the sample is homogeneous. This is not

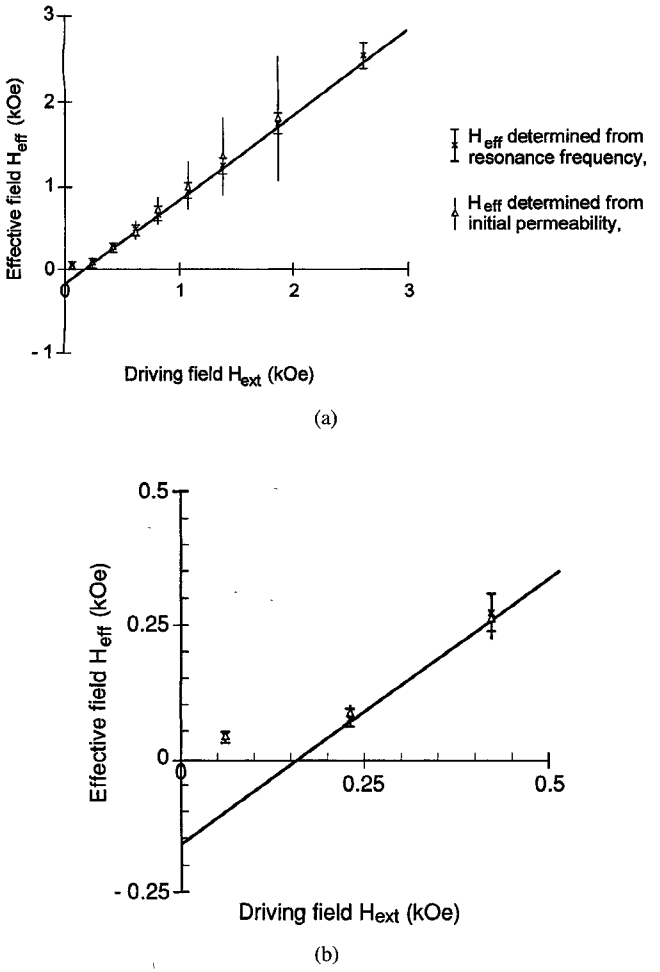

Fig. 12. Effective internal field determined from the measured resonance frequency (crosses) and initial permeability (triangles) on sample A, as a function of external field H_{ext}. The error bars are pictured. The asymptote with slope unity is also represented. (a) Full view. (b) Detail of the low-field region.

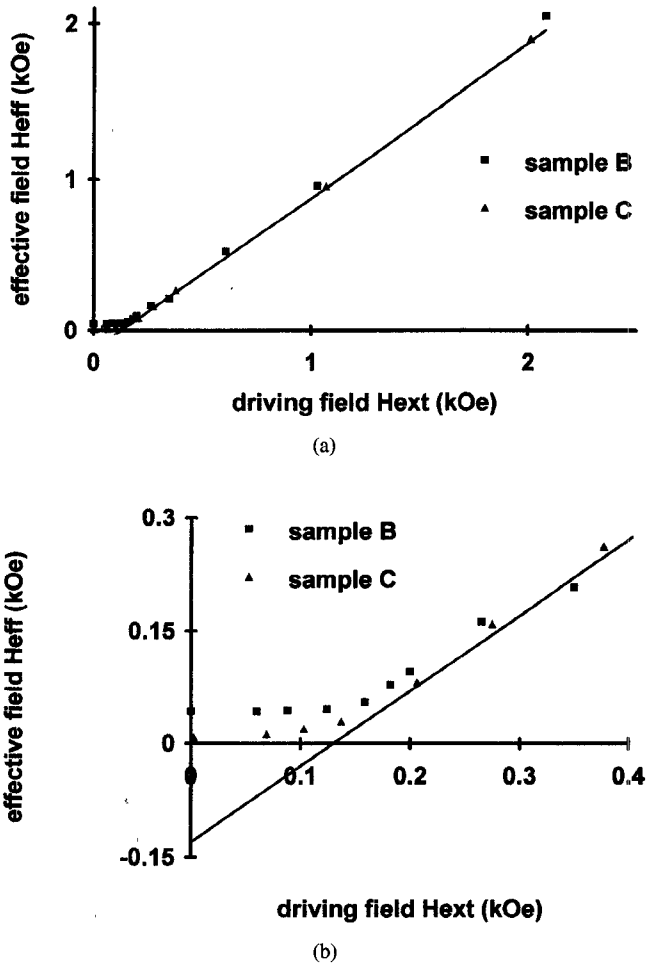

Fig. 13. Effective internal field of samples B and C determined from initial permeability measurements. The asymptote with slope unity is also represented. (a) Full view. (b) Detail of the low-field region.

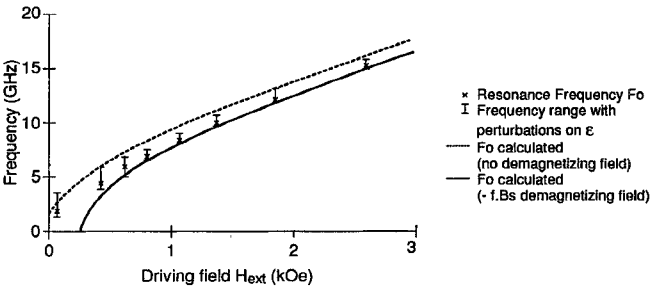

Fig. 14. Resonance frequency F_0 (curve a) and perturbation frequencies on permittivity (curve b) measured on sample A as a function of the external field. Resonance frequencies computed from (4) with $H_{\text{eff}} = H_{\text{ext}}$ (curve c) or $H_{\text{eff}} = H_{\text{ext}} - f_c 4\pi M_s$ (curve d) are also represented.

strictly the case in our samples, because demagnetizing field inhomogeneities induce permeability inhomogeneities. The small perturbations seen on the ϵ' and ϵ'' curves (see Figs. 4 and 6) may be connected with experimental errors due to these inhomogeneities.

To support this view, the characteristic frequencies of the perturbations on the permittivity is plotted on Fig. 14, on the same graph as the permeability resonance frequencies F_0. Resonance frequencies calculated using (4) and either $H_{\text{eff}} = H_{\text{ext}} + H_k$ or $H_{\text{eff}} = H_{\text{ext}} + H_k - f_c 4\pi M_s$ are also plotted. The observed resonance frequencies and perturbation frequencies are clearly within the calculated limits. This shows that the field inhomogeneities within the sample due to demagnetizing effects are less than $f_c 4\pi M_s$. For external fields large compared to $f_c 4\pi M_s$, the samples are mostly saturated and the demagnetizing field H_d no longer depends on the external field H_{ext}. Under these conditions, (6) predicts a linear dependence with slope unity of H_{eff} with H_{ext} at high field, which is actually observed on Figs. 12 and 13.

In the low field regime on samples A and B, H_{eff} is hardly affected by the external field, even for H_{ext} several times larger than H_k. This is coherent with our assumption that domain wall movements permeability is negligible. This also supports the fact that the gyromagnetic resonance frequency of a thin film with in-plane anisotropy is the same in the unsaturated and saturated regime [19].

The samples with low permeability in the demagnetized state (sample C and D) would be expected to have a permeability equal to unity in the absence of external field. This is not strictly the case (see Fig. 5 and 7), though permeability levels are small, especially in the case of sample D. They exhibit a

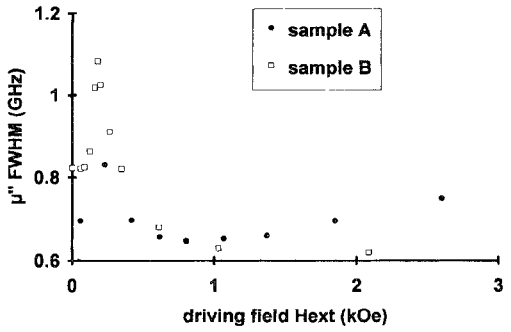

Fig. 15. Gyromagnetic resonance peak FWHM ΔF as a function of the external field for samples A and B.

permeability enhancement at low field. This can be attributed to the field-induced rotation of the local magnetization. When a field comparable to the anisotropy field is exerted along the hard axis, the magnetization rotates from the orthoradial easy direction to the hard direction along the torus axis. It is believed that the evolution of H_{eff} at low H_{ext} should be interpreted in the same terms as conventional transverse susceptibility measurements [20], with small demagnetizing effects in addition. The high field evolution is similar to that of samples with high permeability in the demagnetizing state, except that the contribution of the anisotropy field to the effective field in (6) is $-H_k$ instead of $+H_k$. However, the two-peak high field behavior of sample C [see Fig. 5(b)] remains unexplained.

3) Gyromagnetic Linewidth: The damping parameter is a phenomenological term in the gyromagnetic resonance models. Our experiments allow its determination as a function of the external field. Fig. 15 pictures the gyromagnetic linewidth ΔF with external field for samples A and B. Sample C exhibits two separate peaks, especially at high field. For that reason, both low HWHM and FWHM are represented on Fig. 16.

It appears quite clearly on Fig. 15 that the gyromagnetic linewidth reaches a maximum at a few hundred Oersted. This is interpreted as the effect of an inhomogeneous broadening of the resonance, due to increasing demagnetizing field inhomogeneities. However, when the external field further increases, the effect of a given inhomogeneity on H_{eff} leads to a smaller dispersion on the resonance frequency, as can be seen on (4b). It appears that ΔF is nearly constant at high field, and close to the zero field value. As a consequence, the phenomenological damping parameter of the Bloch model should be expressed in terms of ΔF rather than in term of the dimensionless relative damping parameter $\beta = (\Delta F/F^*)$. These observations can be related to previous studies of gyromagnetic permeability under stress performed on similar ferromagnetic materials [21]. It has been shown that magnetostrictive effects can induce large frequency shifts of the gyromagnetic resonance frequency, but that the linewidth is little affected by this change.

4) Skin Effect: Skin effect has been neglected in the calculations, and (1) has been used to relate the permeability of the composite to that of the layer. However, (2) shows that a small contribution of skin effect can be expected. In the case of sample A, neglecting skin effect leads to an error on $\mu''_{\max}$ of 5 to 7%. The determination of the intrinsic permeability can be made from that of the composite [6] by numerical inversion of (2), but this is no longer valid in the case of an inhomogeneous broadening. For that reason, it was preferred to discuss our results using the permeability of the composite rather than the intrinsic permeability of the layer.

Skin effect at a given frequency below the resonance frequency decreases when the external field increases, because the permeability gets lower. However, it can be shown easily from (4) that the C_c corrective factor of (2) at the resonance frequency F^* is nearly independent of the external field if ΔF remains constant, provided H_{eff} is small compared to $4\pi M_s$.

5) Reciprocity: It is well known that ferrimagnetic materials under magnetic field are nonreciprocal materials [22]. Their permeability is given by a nondiagonal tensor [23]. In the present investigation permeability and permittivity measurements were carried with incident wave coming from one port of the analyzer and then from the other port. However, the measurements did not differ significantly depending on the propagation direction. No measurable nonreciprocal effect has been found.

In the case of saturated ferromagnetic thin films, the diagonal elements are given by (4), and there are small off-diagonal elements. In the Bloch–Bloembergen formulation, the ratio of the off-axis element $\chi_{h,p}$ on the hard axis susceptibility element $\chi_{h,h}$ writes

$$\frac{\chi_{h,p}}{\chi_{h,h}} = \frac{F}{\gamma(H_{\text{eff}} + 4\pi M_s).}$$

Since $\gamma 4\pi M_s$ is larger than 22 GHz, it is clear that the off-diagonal susceptibility component is small in the investigated frequency range. This may account for the fact that no measurable nonreciprocal effect has been found in the LIFE samples. Besides, in the presence of such effects, it is not clear what can be observed due to the few modes that can propagate in the coaxial line.

C. Antireflection Behavior

The previous theoretical development allows a deeper insight in the antireflection termination capabilities of LIFE materials. A striking feature of the LIFE material used as tuneable antireflection termination is that its peak frequency can be shifted over a frequency decade, while the maximum absorption remains large (see Fig. 8). The absorbing conditions for the termination in the $\mu'' \gg \epsilon'$ limit are [24]

$$\mu' = \frac{\epsilon'}{3} \tag{8a}$$

$$e = \frac{c}{2\pi\mu'' F} \tag{8b}$$

where e is the LIFE thickness, and c the celerity of light.

Since ϵ' is close to three, (8a) indicates that the absorption frequency is very close to the phase resonance frequency F^* defined by $\mu'(F^*) = 1$. From (2) and (4) it is clear that

$$\mu''(F^*) = \frac{1}{F^*}\frac{f(\gamma 4\pi M_s)^2}{\Delta F}\left(1 + \frac{H_{\text{eff}}}{4\pi M_s}\right) \tag{9}$$

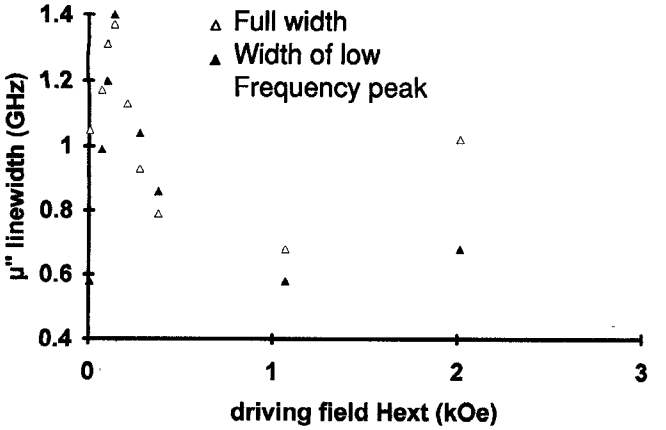

Fig. 16. Gyromagnetic resonance linewidth as a function of the external field for sample C. Full triangle picture twice the low half width at half maximum and open triangles represent the full width at half maximum.

and from (8b)

$$e = \frac{c\Delta F}{2\pi f(\gamma 4\pi M_s)^2} \frac{1}{\left(1 + \dfrac{H_{\text{eff}}}{4\pi M_s}\right)}. \tag{10}$$

If $H_{\text{eff}} \ll 4 \cdot \pi \cdot M_s$ and if ΔF is independent of the external field, the optimal thickness e for the antireflection termination is independent of the external field. Under the same assumptions, it is possible to show from (2) and (9) that skin effect hardly affects this result. The variation of $\mu''(F^*)$ as $1/F^*$ predicted by (9) is illustrated on Fig. 17. The fact that the maximum attenuation of antireflection termination made of sample C degrades at high field (Fig. 9) may be related to the variations of the linewidth ΔF with the external field (see Fig. 16).

D. Transmission Behavior

The very low S_{11} levels obtained at 230 Oe up to 1 GHz [see Fig. 11(a)] are connected to the condition $\mu = \epsilon$ which is very nearly met on this frequency range. A nonmagnetic sample with the same permittivity and thickness as sample B would exhibit S_{11} of about -26 dB, while the observed reflection S_{11} at 230 Oe is lower than -50 dB at this frequency.

The S_{12} properties exhibit also large changes with the exerted field. However, no effort has been made to adjust sample thickness so that large extinction ratios are obtained. Besides, though nearly all the energy penetrates in the sample (S_{11} is small), there are still some dielectric losses that limit the transparency of the sample. It is believed that further work may lead to highly transparent to highly absorptive tuneable material. In contrast with most highly transparent structures, this result is not obtained with half-wave frequency matched samples, but with intrinsic low impedance materials with potential wide band characteristics.

VI. Conclusion

We presented the properties of LIFE in the 0.1 to 18 GHz range under static magnetic field. These materials exhibit large permeability levels, with a resonance frequency that

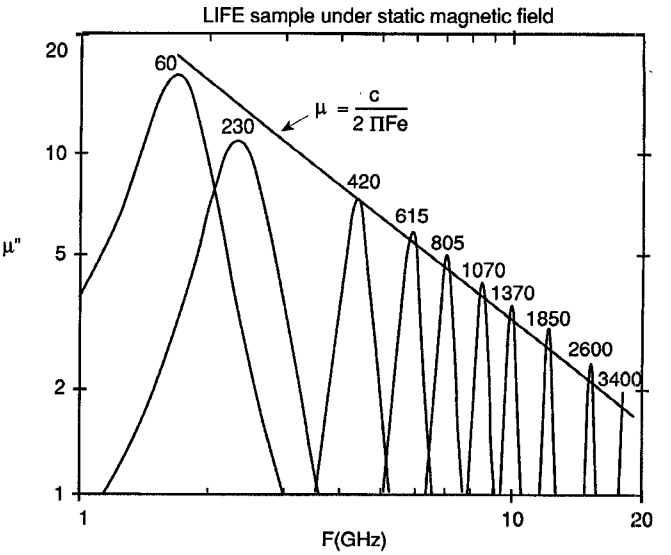

Fig. 17. Permeability of sample A as a function of the frequency for the different external fields (indicated in Oe) in a log-log scale. A line corresponding to a $1/F$ variation is also pictured.

varies with the external magnetic field. The evolution of the permeability with the external field is well described by a classical gyromagnetic model. The gyromagnetic linewidth has been investigated as a function of the external field. It remains nearly constant with the field, except for some inhomogeneous broadening due to demagnetizing effects. It was shown that LIFE materials exhibit a reciprocal behavior.

We presented some examples of potential applications such as switchable or tuneable antireflection terminations, modulators, phase shifters, or high index impedance-matched materials. All these properties are valid only for the fundamental mode of the coaxial line, because LIFE materials are anisotropic and exhibit their high impedance characteristics only for one polarization or propagation mode. It seems that similar operations would be possible with LIFE materials adapted to single-mode rectangular wave guides.

LIFE materials exhibit large permeabilities, due to the high saturation magnetization of the film and to the LIFE geometry. On the other hand, the low ferromagnetic volume fraction in the material induce small demagnetizing effects. This is a key feature to obtain well-defined field-induced frequency shifts. The unique combination in LIFE material of high permeability and small demagnetizing effects is valuable for applications as tuneable material.

Acknowledgment

The authors would like to thank C. Boscher, G. Nouhaut, and C. Couderc for their contribution to thin film deposition and characterization. They are also grateful to Y. Héry, E. Capelle, and M. Houdayer for their support.

References

[1] P. Butvin, B. Butvinova, and J. Novak, "Using metallic glasses for chokes cores," *IEEE Trans. Magn.*, vol. 30, p. 493, 1994.
[2] M. Hayakawa, "Characteristics of soft magnetic thin films for magnetic head core application," *J. Magn. Magn. Mater.*, vol. 134, p. 287, 1994.

[3] R. M. Walser, "A study of thin film magnetodielectrics," Ph.D. dissertation, Univ. of Michigan, 1967.
[4] L. Olmedo, G. Chateau, C. Deleuze, and J. L. Forveille, "Microwave characterization and modelization of magnetic granular materials," *J. Appl. Phys.*, vol. 73, pp. 6992–6994, 1993.
[5] O. Acher, P. M. Jacquart, J. M. Fontaine, P. Baclet, and G. Perrin, "High impedance anisotropic composites manufactured from ferromagnetic thin films for microwave applications" *IEEE Trans. Magn.*, vol. 30, p. 4533, 1994. O. Acher, P. M. Jacquart, J. M. Fontaine, P. Baclet, G. Perrin and P. LeGourrierc, "Composites anisotropes à forte perméabilité et faible permittivité en hyperfréquences," Proc. 3rd Journées de Caractérization Microondes et Matériaux," Brest, 1994.
[6] O. Acher, J. L. Vermeulen, P. M. Jacquart, J. M. Fontaine, and P. Baclet, "Permeability measurement on ferromagnetic thin films from 50 MHz up to 18 GHz," *J. Mag. Magn. Mat.*, vol. 136, p. 269, 1994.
[7] Born and Wolf, *Principle of Optics*. New York: Pergamon.
[8] S. M. Rytov, "Electromagnetic properties of a finely stratified medium," Sov. Phys. JETP, vol. 2, pp. 466–475, 1956.
[9] G. Mazé, thèse de l'université de Bordeaux, 1991.
[10] A. M. Nicholson and G. F. Ross, *IEEE Trans. Instrum. Meas.*, vol. 17, p. 395, 1968. Hewlett Packard product note no. 8510-3.
[11] A. M. Clogston, "Reduction of skin effect losses by the use of laminated conductors," *Bell Syst. Tech. J.*, vol. 30, 1951, pp. 491–529.
[12] G. Perrin, P. Baclet, J. M. Fontaine, E. Capelle, and O. Acher, "Influence of magnetron sputtering parameters on soft ferromagnetic thin films deposited onto continuously transported thin polymer substrates," supplément à la revue *"Le vide: Science, technique et applications,"* no. 275, pp. 256–259, 1995.
[13] M. Naili and G. Suran, "The mechanism governing the formation and magnitude of the induced anisotropy Ku in amorphous CoZrM and CoZrPt thin films," *J. Magn. Magn. Mater.*, vol. 135, 1994, p. 1441.
[14] A. Materne, thèse de l'université de Grenoble, 1989.
[15] J. C. Peuzin and J. C. Gay, *Acte des Journées d'étude sur la Caractérization Microonde des Matériaux Absorbants*. Limoges, 1991, p. 75.
[16] A. Verdier, N. Bardy, and J. P. Prulhière, "Validation of a broadband measurement method of complex permeability and permittivity with a network analyzer, estimation of the measurement accuracy," in *Proc. Conf. Precision Electromagnetic Measurements*, Paris, June 9–12, 1992.
[17] N. Bloembergen, "On the ferromagnetic resonance in nickel and supermalloy," *Phys. Rev.*, vol. 78, 1950, pp. 572–580.
[18] J. C. Mallinson, "Damped gyromagnetic precession," *IEEE Trans. Magn.*, vol. 23, p. 2003, 1987.
[19] Stuijts and Wijn, *Rev. Tech. Phil.*, vol. 19, p. 221, 1957.
[20] H. Hoffman, G. Heller, and F.-H. Kammerer, "Uniaxial and local anisotropies in amorphous thin CoZr films," *IEEE Trans. Mag.*, vol. 23, p. 2731, 1987.
[21] O. Acher, J. L. Vermeulen, A. Lucas, P. Baclet, J. Kazandjoglou, and J. C. Peuzin, "Direct measurement of permeability up to 3 GHz of Co-based alloys under tensile stress," *J. Appl. Phys.*, vol. 73, pp. 6162–6164, 1993.
[22] S. K. Koul and B. Bhat, "Microwave and millimeter wave phase shifters," vol. 1. Boston: Artech House, 1991.
[23] D. Polder, "On the theory of ferromagnetic resonance," *Phil. Mag.*, vol. 40, p. 99, 1949.
[24] P. Hartemann and M. Labeyrie, "Absorbants d'ondes électromagnétiques," *Revue Tech. Thomson CSF*, vol. 19, 1987, p. 413.

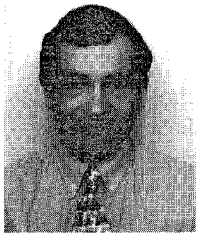

Olivier Acher was born in Paris, France, in 1963. He graduated from the Ecole Polytechnique in 1986, and received the Diplôme d'Etude Approfondie of Solid State Physics from the University of Paris XI in 1987. He received the Ph.D. degree in 1990.

From 1986 to 1990 he was with the Thomson-CSF Laboratoire Central de Recherche, working on the epitaxy of III-V semiconductors and on their in-situ characterization by reflectance anisotropy measurements, in a collaboration with the LPICM at the Ecole Polytechnique. He participated in building the first commercially available reflectance anisotropy setup with the Jobin Yvon company. In 1990, he has joined the CEA at Bruyères-le-Chatel. At present, his main research interest is in static and dynamic properties of ferromagnetic materials. He has authored or co-authored 33 papers.

Dr. Acher was awarded an E-MRS Young Scientist Award in 1989 and a IBM-France prize in material science in 1990. He holds six patents.

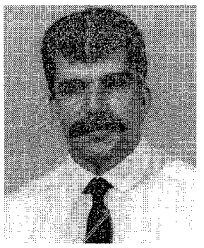

Pierre Le Gourriérec was born in Pontivy, France, in June 1960. He received the Dipl. Ing. degree from Conservatoire National des Arts et Métiers in 1989.

Since 1981, he has been in the Atomic Energy Commission. From 1981 to 1989 he worked on the Ionic Cyclotron Resonance experiment at the Centre d'Etudes Nucléaires de Saclay. Since 1989 he has been working at the Centre d'Etudes de Bruyères-Le-Châtel.

Géraldine Perrin was born in Grenoble, France, on August 12, 1970. She received the engineer degree in 1993 from the ENSPG, Grenoble. Since 1993, she has been working toward the Ph.D. degree at the Commissariat à l'Energie Atomique (CEA), Bruyères-le-Châtel.

Her current research interest is in the field of high frequency properties of magnetic thin films.

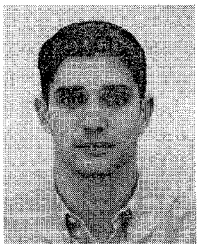

Philippe Baclet was born in 1968 in Pont-l'Abbé, France. He graduated from the ESPCI (Ecole Supérieure de Physique et de Chimie Industrielle de la Ville de Paris) in 1991, and received the Diplôme d'Etude Approfondie of Material Science from the University of Paris VI in 1991.

In 1991, he joined the CEA at Bruyères-le-Chatel. At present, his main research interest is surface treatments (PVD, electrochemical coatings) and analysis. He has authored or co-authored eight papers.

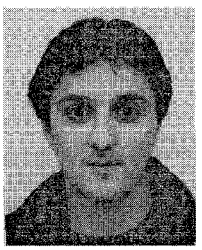

Olivier Roblin was born April 1971. He graduated from SUPELEC in 1994.

He is currently involved in electronics and computer science research.